Dimerization of PHGDH *via* the catalytic unit is essential for its enzymatic function

Hanyu Xu[1,‡], **Xiaoyu Qing**[1,‡], **Qian Wang**[2], **Chunmei Li**[3], and **Luhua Lai**[1,3,*]

From the [1]*BNLMS, Peking-Tsinghua Center for Life Sciences at College of Chemistry and Molecular Engineering, Peking University, Beijing, China;* [2]*State Key Laboratory of Natural and Biomimetic Drugs, School of Pharmaceutical Sciences, Peking University, Beijing, China; and* [3]*Center for Quantitative Biology, Academy for Advanced Interdisciplinary Studies, Peking University, Beijing, China*

Edited by Ruma Banerjee

Human D-3-phosphoglycerate dehydrogenase (PHGDH), a key enzyme in *de novo* serine biosynthesis, is amplified in various cancers and serves as a potential target for anticancer drug development. To facilitate this process, more information is needed on the basic biochemistry of this enzyme. For example, PHGDH was found to form tetramers in solution and the structure of its catalytic unit (sPHGDH) was solved as a dimer. However, how the oligomeric states affect PHGDH enzyme activity remains elusive. We studied the dependence of PHGDH enzymatic activity on its oligomeric states. We found that sPHGDH forms a mixture of monomers and dimers in solution with a dimer dissociation constant of ∼0.58 μM, with the enzyme activity depending on the dimer content. We computationally identified hotspot residues at the sPHGDH dimer interface. Single-point mutants at these sites disrupt dimer formation and abolish enzyme activity. Molecular dynamics simulations showed that dimer formation facilitates substrate binding and maintains the correct conformation required for enzyme catalysis. We further showed that the full-length PHGDH exists as a dynamic mixture of monomers, dimers, and tetramers in solution with enzyme concentration-dependent activity. Mutations that can completely disrupt the sPHGDH dimer show different abilities to interrupt the full-length PHGDH tetramer. Among them, E108A and I121A can also disrupt the oligomeric structures of the full-length PHGDH and abolish its enzyme activity. Our study indicates that disrupting the oligomeric structure of PHGDH serves as a novel strategy for PHGDH drug design and the hotspot residues identified can guide the design process.

Cellular metabolism is the basis of biological activities (1). Amino acid synthesis and metabolism provide building blocks and energy to meet the demands of cell growth and tackle the challenge of oxidative stress (2). As a nonessential amino acid, serine participates in the synthesis of nucleotides, lipids, other amino acids, antioxidants, and cofactors, which plays critical roles in a number of biosynthetic and signaling pathways in addition to serving as a major donor of one-carbon units (3). L-Serine is also the immediate precursor of D-serine, a neurotransmitter that relies on *de novo* serine synthesis due to the poor transport of plasma serine across the blood–brain barrier (4). Human D-3-phosphoglycerate dehydrogenase (PHGDH) is the first and rate-limiting step of *de novo* serine synthesis, converting the 3-phosphoglycerate (3-PG) generated from glycolysis into serine precursor 3-phosphohydroxypyruvate (3-PHP) coupled with NAD$^+$. This product is subsequently converted to 3-phosphoserine by the 3-phosphoserine aminotransferase (PAST1) and then to L-serine *via* 3-phosphoserine phosphatase (PSPH) (5). PHGDH not only provides serine and one-carbon units to support cell growth, but also coordinates the utilization efficiency of one-carbon unit from different sources to promote tumorigenesis (3, 6). As a metabolic enzyme, PHGDH amplification is found to be involved in many cancers such as breast cancer (7, 8), melanoma (8), lung cancer (9), glioma (10), Ewing sarcoma (11), pancreatic cancer (12), and renal cell carcinoma (13). Furthermore, high expression level of PHGDH was found to be related to tumor resistance to chemotherapies (14–16). For instance, PHGDH is identified as an attractive target to overcome tyrosine kinase inhibitor (TKI) drug resistance in hepatic cell carcinoma (HCC) by Genome-wide CRISPR/Cas9 knockout library screen and chemical genetics (17). Recently, Ngo *et al.* (18) demonstrated that PHGDH is a major determinant of brain metastasis in multiple human cancer types and preclinical models and explored the possibility of PHGDH inhibitors for treating brain tumor metastasis. These findings suggest that targeting PHGDH provides a promising anticancer and drug resistance approach (19).

PHGDH belongs to the SerA subset of D-isomer-specific 2-hydroxyacid-dehydrogenase (2HADH) family that catalyzes the stereospecific reductions of 2-keto acids to corresponding 2-hydroxy acids (20). D-3-phosphoglycerate dehydrogenases (PGDHs) expressed in various organisms are grouped into three types based on their domain arrangement. All the three types of PGDHs have a common catalytic unit containing the substrate-binding domain and the cofactor-binding domain. Type III PGDH from *Entamoeba histolytica* with only the catalytic unit adopts a dimeric configuration (21). PHGDH belongs to the most complex type I PGDHs, which contain two additional regulatory

domains, the ACT (aspartate kinase-chorismate mutase-tyrA prephenate dehydrogenase) and ASB (allosteric substrate binding) domains (5). The ACT domain plays its role in the feedback inhibition by L-serine in bacteria, while all mammalian enzymes so far studied have lost this ability (22). The ASB domain functions as a substrate-binding regulatory site in *Mycobacterium tuberculosis* (23). However, the functions of these two regulatory domains of PHGDH remain elusive and the full-length structure of PHGDH is currently unavailable. The only full-length type I PGDH structure (PDB code: 1YGY) solved was that from *M. tuberculosis*, which forms tetrameric structure (23). Although the full-length PHGDH is not currently available, the structure of its catalytic unit without the two regulatory domains has been solved as a dimer (sPHGDH, PDB codes: 2G76, 5N6C, and 6CWA). In the 2G76 structure, the carboxylate moiety of the substrate analog (D-malate, MLT) forms hydrogen bonds with Arg54 and Ser55 and Arg135' from the other monomer (24). Unlike the substrate analog, the NAD$^+$ interacts only within one monomer in the 5N6C structure of sPHGDH (25). The truncated form of PHGDH retains 75% catalytic activity compared with the full-length PHGDH (25), which was presumed to function as a tetramer (26).

Dimerization or oligomerization is widely used by natural proteins to increase stability and regulate enzyme activity (27, 28). In the dimeric structure of sPHGDH with 3-PG and NAD$^+$ (PDB code: 6CWA), R135' from the other protomer was found to interact with the phosphate group of 3-PG (29), implying that the dimerization of the catalytic unit may be essential. Three pathogenic variants (R135W, G140R, and R163Q) responsible for PHGDH deficiency and Neu–Laxova syndrome 1 (NLS1) diseases locate at the sPHGDH dimer interface. It was reported that R135W resulted in a moderate decrease of enzyme activity (30). Moreover, an interfacial mutation E108A of *E. histolytica* PGDH (EhPGDH) caused dimer dissociation and reduced enzyme activity, suggesting that dimer interface plays a crucial role in the stability of the protein and a complete dimer is required for the optimal enzymatic activity of EhPGDH (31). W139 in *Escherichia coli* PGDH (corresponding to position 133 in human PHGDH), which sits at the bottom of the catalytic site of the adjacent subunit, plays a critical role in maintaining the oligomeric state of the enzyme as well as the integrity of the catalytic site (32). W139G of *E. coli* PGDH weakens the subunit/subunit contact and is 600-fold less active. It appears to be in equilibrium between a tetrameric and a dimeric form, and the dimeric species were proposed to be mediated by interactions of the regulatory domains (33). However, there is no suggestive evidence about the relationship between the dimerization or oligomerization and the activity of PHGDH.

Here, we addressed this question by analyzing the solution behavior and biophysical properties of both the catalytic unit and the full-length wild-type PHGDH and variants. We computationally identified hotspot residues at the dimer interface of sPHGDH and studied the oligomeric state and catalytic activity of corresponding mutants. We showed that sPHGDH exists as a monomer and dimer mixture and only the dimeric form is catalytically active. Mutants that disrupt the dimeric structure of sPHGDH showed reduced enzyme catalytic activity. We also showed that full-length PHGDH exists as a monomer, dimer, and tetramer mixture in solution and their ratios vary with enzyme concentration. We demonstrated that dimerization is required to maintain the enzyme activity of PHGDH. Targeting the dimerization of PHGDH provides an alternative approach for PHGDH inhibitor design and the interface hotspots we identified serve as a guideline for interfacial inhibitor design.

Results

Enzyme activity of sPHGDH depends on its dimer state

The catalytic unit of PHGDH (sPHGDH, 1–307) containing the cofactor-binding domain and the substrate-binding domain, forms a homodimer in the crystal structure (24). Whether this dimer is essential for the catalytic activity is not fully understood. We expressed and purified sPHGDH, studied its oligomeric states and concentration-dependent catalytic activity in solution. Analytic ultracentrifugation (AUC) sedimentation velocity analysis revealed two peaks (~2.4S and 3.9S), corresponding to the monomeric and dimeric state of sPHGDH (Fig. 1A). The dimer and monomer peak ratio displayed concentration dependent increase with the 1:1 ratio at about 1 μM. We further measured sPHGDH catalytic activity at different enzyme concentrations with excessive substrate and cofactor. While the K_m did not change much (Fig. S1), the $k_{cat, app}$ increased abruptly along with the increase of the total enzyme concentration (Fig. 1B) and the dimer proportion. Assuming that there is an equilibrium between the monomer and dimer and both of them are active, we derived their catalytic parameters according to the following equations.

$$K_d = \frac{[M][M]}{[D]} \quad (1)$$

$$[E] = [M] + 2[D] \quad (2)$$

$$V = k_{cat,app}[E] = k_{cat,mono}[M] + k_{cat,dimer}[D] \quad (3)$$

$$V = k_{cat,mono}\frac{\sqrt{K_d^2 + 8K_d[E]} - K_d}{4} + k_{cat,dimer}\frac{4[E] + K_d - \sqrt{K_d^2 + 8K_d[E]}}{8} \quad (4)$$

Here [M], [D], and [E] refer to the monomer, the dimer, and the total concentration of PHGDH, respectively. K_d is the apparent dissociation constant of the dimer. $k_{cat, app}$ is the apparent catalytic constant. $k_{cat, dimer}$ and $k_{cat, mono}$ are the
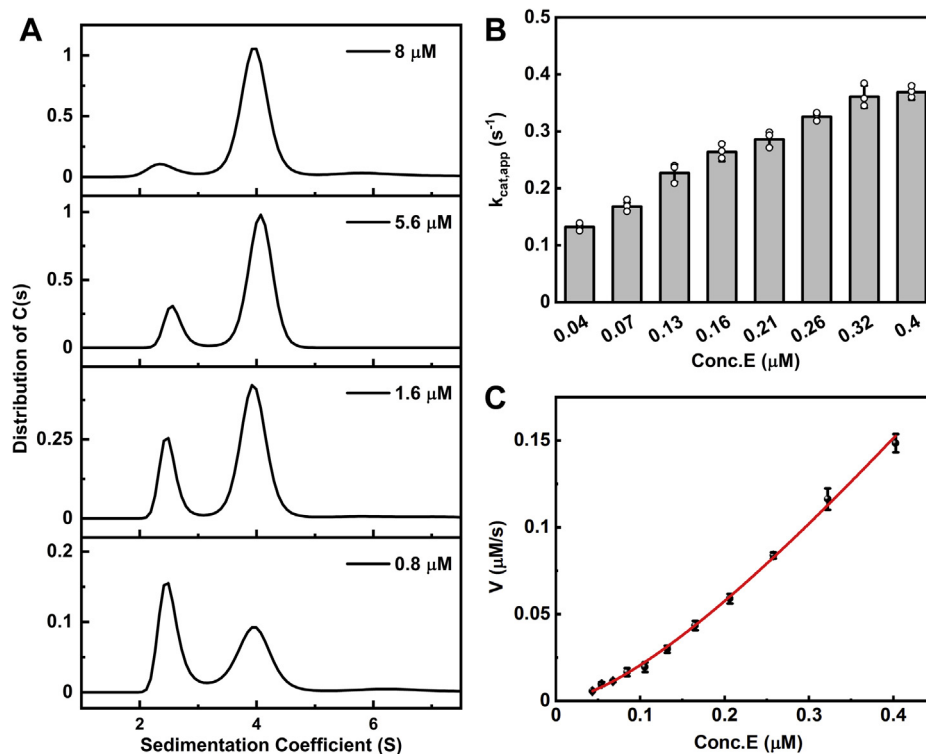
Figure 1. Enzyme activity of sPHGDH depends on the dimer structure. *A*, sedimentation coefficient distribution c(s) profile of sPHGDH WT at the indicated concentration. *B*, the catalytic rate constant $k_{cat, app}$ ($k_{cat, app} = V_{max}/[E]$, V_{max} = maximum reaction rate, [E] = total enzyme concentration) increases with the increased enzyme concentration. *C*, enzyme activity of sPHGDH at different concentrations with excessive substrate and cofactor (3 mM 3-PG, 3 mM NAD+). The curve is fitted by *Equation 4*. *Error bars* represent SD (n ≥ 3).

catalytic constants of the monomer and the dimer, respectively. By fitting the enzyme activity data at different [E] values using *Eq.4*, the $k_{cat, mono}$ was deduced as 0.04 s^{-1}, the $k_{cat, dimer}$ was 1.62 s^{-1}, and the K_d was 0.58 μM (Fig. 1C). The $k_{cat, dimer}$ is 40-fold to $k_{cat, mono}$, indicating that the monomer contributes little to enzyme activity. These observations suggest that sPHGDH dimeric assembly is essential for its catalytic activity.

Analysis of hot spot residues at the dimer interface of sPHGDH

We have shown that the dimer structure of sPHGDH is essential for its catalytic activity. In order to identify mutations that can perturb the dimer structure, we performed computational alanine screening and structural analysis with the sPHGDH structure (PDB: 2G76, DOI: 10.2210/pdb2G76/pdb) to identify putative hot spots using the FoldX method and molecular dynamics (MD) simulations (34–36).

As the interface consists of 122 interfacial residues contributed equally by the two subunits, we used the alanine screening method implemented in FoldX 5 (the PSSM module) as the primary screening tool to unravel key residues (36, 37). We found 14 strong destabilizing residues (effective ΔΔG ≥ 1.82 kcal/mol), including E108, L109, R119, I121, T125, M128, K129, W133, L143, F262, R270, E290, and R294. We also detected several weak destabilizing residues including S105, M115, R163, V273, I279, and L284. Subsequently, we subjected all these predicted strong and weak destabilizing residues to MD simulation-based alanine screenings to further distinguish energetically hot spots. In addition, we also carried

out MD simulations for the three naturally occurring variants, including R135 W, G140 R, and R163Q (Fig. 2A), to evaluate their effects on dimerization. Each of the sPHGDH protein and interfacial variants underwent three 200 ns MD production simulations, and the binding free energies between the two protomers forming the dimer were calculated using the MM-GBSA method implemented in AMBER16 (38).

As shown in Figure 2B, listed mutants significantly weakened the binding free energies as compared with the WT sPHGDH structure. Effective ΔΔG of substitutions including E108A, R119A, I121A, T125A, M128A, K129A, W133A, R135W, G140R, R163Q, and I279A exceeded 10 kcal/mol. Furthermore, we found that five out of the ten predicted key residues including E108, R119, and W133 are highly conserved, while I121 and I279 are moderately conserved according to the sequence alignment of the SerA subfamily homologs. In addition, these five residues are also structurally conserved and fully buried in the interface among the SerA subfamily *via* structure-based sequence alignment with known PGDH structures (PDB codes: 2G76, 4NJO, 1YBA, 1YGY, 3K5P, 1WWK, and 2EKL) (Fig. S2) (20, 23, 39, 40). Protein–protein interaction studies have suggested that hot spots are likely to be structurally conserved residues and are organized in high packing density regions. We therefore selected these five key residues together with the three naturally occurring variants (R135W, G140R, and R163Q) as putative hot spots for further experimental validation (41–43). It is noteworthy that the residues predicted to contribute significantly to the
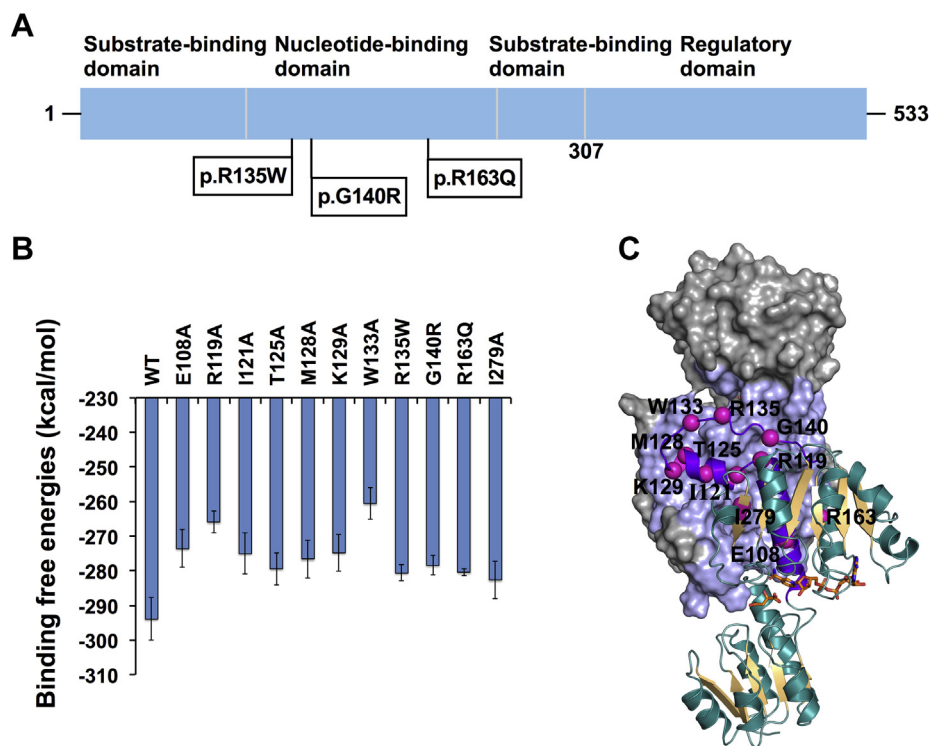
Figure 2. Putative hot spot analysis of the dimer interface in sPHGDH. *A*, the full-length PHGDH is composed of 533 amino acids, in which the catalytic unit (sPHGDH, amino acids 1–307) consists of the substrate-binding and nucleotide-binding domains, with the three naturally occurring variants indicated. *B*, calculated binding free energies for the WT sPHGDH and the interfacial mutants. *C*, predicted energetic hot spots (shown as *pink spheres*) are mainly located at the region of the dimer interface containing a core helix and the dimerization loop (highlighted as *purple*).

energetics of dimer formation are mainly located at a region consisting of a core helix (aa: 102–119) and an interfacial loop referred to as the dimerization loop (aa: 120–145) (Fig. 2C) (44). The core helix possessing more hydrophobic residues is fully buried in the interface, whereas the dimerization loop contains atoms that retain partial accessibility. Remarkably, the dimerization loop is adjacent to the catalytic loop (aa: 280–288, H283 is the proton donor during catalysis), which provides the active site with a substrate-binding residue (R135) based on a lately solved sPHGDH-complex structure (PDB: 6CWA) (29). These results imply that the dimer interface and subunit contacts might directly participate in the catalytic processes.

Mutations of the sPHGDH interfacial hot spot residues disrupt dimer formation

We expressed and purified the five conserved hot spot mutants (E108A, R119A, I121A, W133A, and I279 A), the three pathogenic mutants (R135W, G140R, and R163Q), as well as R135A. We also purified two active site mutants, R236E (26) and H283A (45), as controls. All the 11 mutants were stably expressed and folded, as shown in the SDS-PAGE gel (Fig. S3A) and CD (circular dichroism) spectra (Figs. S4A and S7). The CD spectra of R135A and R236E are similar to WT sPHGDH, while those of other mutants changed shape to a certain extend at the same concentration (0.5 mg/ml, 16 µM). We further measured the CD spectra of WT sPHGDH at different concentrations. It is interesting that along with the

decrease of its concentration and dimer proportion, the CD spectra of WT sPHGDH became similar to those of other mutants (Fig. S5). We speculate that these spectra changes may be caused by the differences of the dimer and monomer structures and their ratio changes. To further verify this, we performed the CD thermal denaturation experiments (Figs. S6 and S7). Two abrupt changes were found at 222 nm and 208 nm and the corresponding T_m values were 36.2 °C (Figs. S6B) and 45 °C (Fig. S7B), respectively. At 40 °C, sPHGDH WT gave similar spectrum to most mutants (Fig. S6A).We assume that the first T_m revealed the transition of the dimer to monomer state, and the second T_m indicated the unfolding process of the overall structure as sPHGDH basically contains α/β structures. The unfolding T_m of WT sPHGDH and mutants are comparable (Figs. S7 and S8), which did not change significantly, indicating that the mutants are well structured.

We first checked the oligomeric states of the mutants using size-exclusion chromatography (SEC) and chemical cross-linking. In the SEC experiment, all the proteins were eluted as a single, symmetrical peak except R135W that showed two distinct peaks (Fig. S10A) at the concentration of 16 µM. Remarkably, all the five conserved hot spot mutants, two of the three pathogenic mutants (G140R and R163Q), as well as the active site mutant H283A were eluted with larger retention volumes corresponding to the monomeric state (Fig. 3A and Table S1). R135A and the active site mutant R236E appeared as dimer, while R135W showed one monomer and one dimer
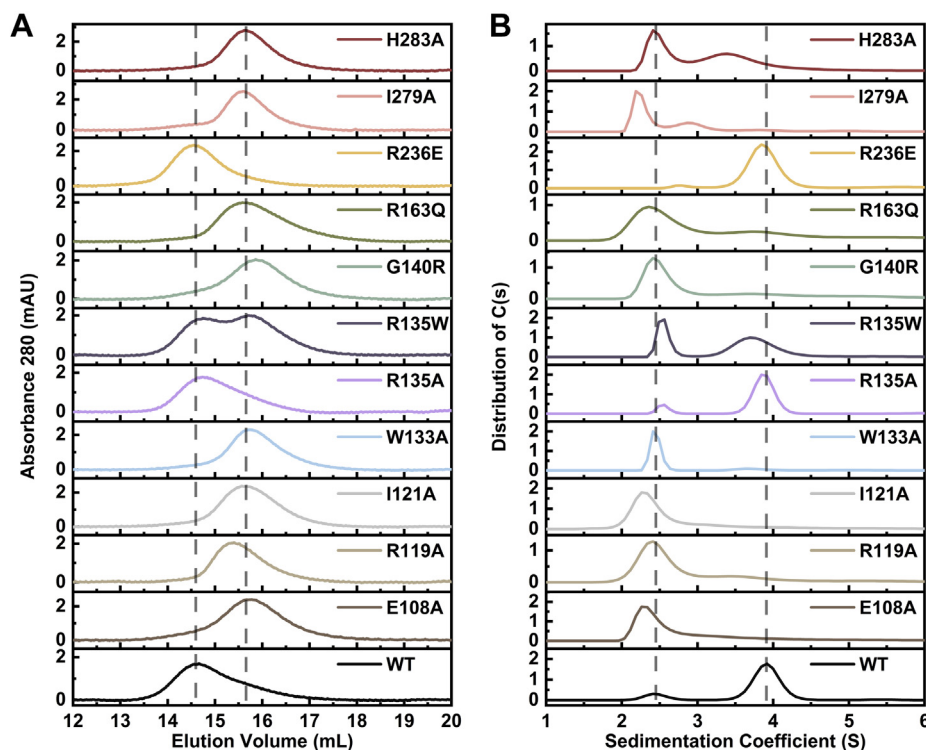
Figure 3. Oligomeric states of the sPHGDH WT and mutants at the concentration of 0.5 mg/ml (16 μM). *A*, size-exclusion chromatograms of sPHGDH and mutants. *B*, the stack map of sedimentation coefficient distribution c(s) profile of sPHGDH and mutants.

peak with similar intensity. We also carried out chemical cross-linking experiment for all the mutants as well as WT protein (Fig. S11, *A* and *B*), using bis-sulfosuccinimidyl suberate (BS3) as cross-linker, which are consistent with the SEC results. We further verified the oligomeric state of the mutants using analytic ultracentrifugation sedimentation velocity analysis. In accordance with the SEC and chemical cross-linking results, R236E and R135A mainly existed as dimer, R135W existed as a monomer and dimer mixture, while all the five conserved interfacial mutants, G140R, R163Q, and H283A mainly existed as monomer states (Fig. 3B and Table S3).

These experimental results are in consistent with our computational analysis. The five conserved hot spot mutants (E108A, R119A, I121A, W133A, and I279A) and the two pathogenic mutants (G140R and R163Q) perturbed the dimer formation completely, while the pathogenic mutant R135W reduced the dimer fraction by about one half. As the substrate analog MLT in one monomer was observed to interact with the R135' residue from the other monomer in the complex structure of sPHGDH, R135 was supposed as a key residue for PHGDH catalysis (30). However, Shaheen *et al.* (46) speculated that the pathogenic mutant R135W might not perturb the overall protein structure and function significantly based on the analysis of structure as there is enough space to accommodate a Trp substitution. Our study showed that R135A did not change the oligomeric state of the sPHGDH and R135W keeps a dimer fraction of about 55%, indicating that the contribution of R135 to the dimerization is limited.

Mutations of the sPHGDH interfacial hot spot residues reduced enzymatic activity

We measured and compared the catalytic activity of all the 11 sPHGDH mutants with the WT protein (sPHGDH). The two active site mutants, R236E and H283A, completely lost activity. The five sPHGDH interfacial mutants, including E108A, R119A, I121A, G140R, and R163Q, showed significant decrease in enzyme activity. Among them, E108A and I121A barely showed observable activity (Figs. 4A and S14). At the concentration of 2.4 μM, the other two interfacial mutants, W133A and I279A, showed slightly noticeable enzymatic activity. R135A kept about 80% activity to the WT and R135W retained about half activity (Fig. 4B). Altogether, the enzyme activity profiles are highly consistent with our dimer interfacial hotspot predictions and the experimental dimer fraction analysis.

We further calculated the kinetic parameters of the enzyme reaction for WT sPHGDH and mutants at the 2.4 μM concentration (Fig. 4, *C* and *D*). $K_{m,3-PG}$ of R135A is about threefold of the WT sPHGDH, while its k_{cat} did not change much (Table 1), indicating that the salt bridges formed by R135'with 3-PG only modestly contribute to substrate binding. With sufficient concentration of 3-PG, the activity of R135A is similar to WT sPHGDH. In contrast, R135W not only showed weakened 3-PG binding ability, but also significantly reduced k_{cat} (about one half). Our study suggests that R135' is not essential to catalysis.
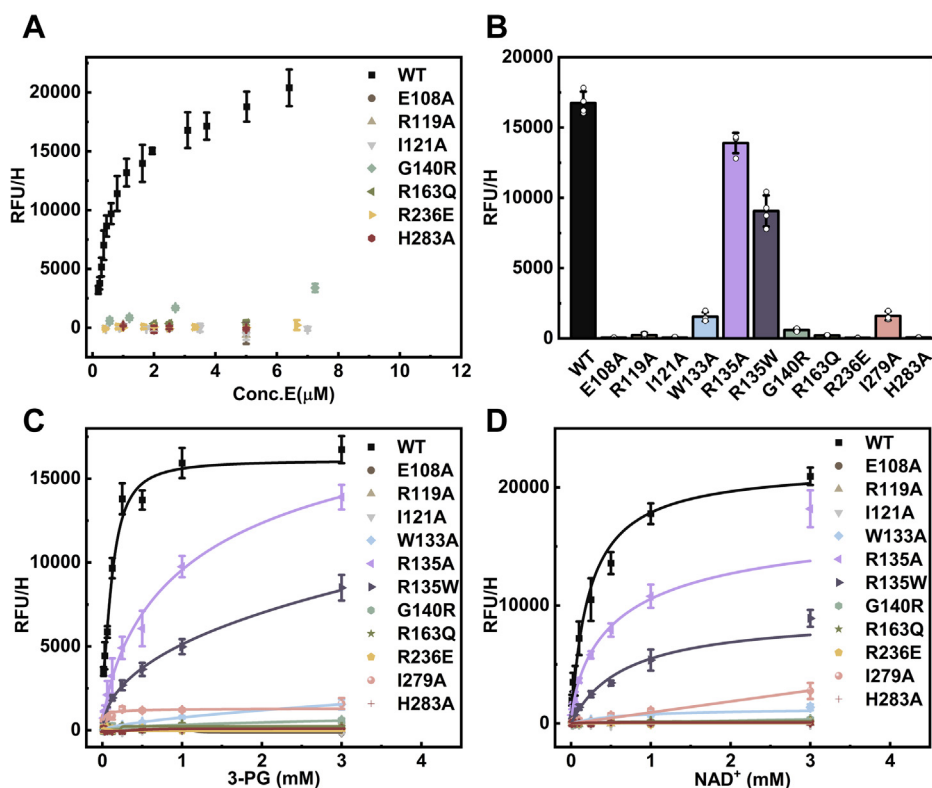
Figure 4. Enzyme activity of sPHGDH and mutants. *A*, enzyme activity of sPHGDH WT and mutants at the indicated concentration. *B*, enzyme activity of 2.4 μM sPHGDH and mutants with 3 mM 3-PG, 1 mM NAD⁺. *C*, the reaction kinetics of 2.4 μM sPHGDH and mutants with 1 mM NAD⁺ at different 3-PG concentrations. *D*, the reaction kinetics of 2.4 μM sPHGDH and mutants with 1 mM 3-PG at different NAD⁺ concentrations. *Error bars* represent SD (n ≥ 3).

The role of the dimeric complex

We have demonstrated the dependence of sPHGDH's enzymatic activity on its dimeric state. How the dimer formation affects the enzyme activity needs to be further explored. We analyzed the dynamic structural properties of the dimeric (with and without a substrate analog, D-malate: MLT) and monomeric structures of sPHGDH by performing long MD simulations (500 ns production run, with three independent repeats).

RMSD and RMSF calculations show that the dimer structure is generally more stable than the standalone monomeric structure in the MD trajectories (Fig. S12*A*). In particular, the

dimerization loop (residues 120–145) and the catalytic loop (residues 280–288) represent the least stable regions in the monomeric trajectories compared with the dimeric forms (Fig. S12*B*). This is in concordance with self-assembly enzyme studies demonstrating that oligomerization is an adaptive strategy to acquire thermal stability (27). On the other hand, dissociation of these intersubunit contacts would lead to significant distortion of the active site configuration as well as the stability of the complex (28, 47, 48).

In addition to enhancing thermodynamic stability, intersubunit interactions may fluctuate into conformations resembling the bound state even in the absence of ligands,

Table 1
Kinetic parameters of the sPHGDH forward reaction coupled with PSAT1

sPHGDH	$K_{m,3-PG}$ (mM)	$k_{cat,\ 3-PG}$ (s⁻¹)	$k_{cat}/K_{m,\ 3-PG}$ (mM⁻¹s⁻¹)	$K_{m,\ NAD+}$ (mM)	$k_{cat,\ NAD+}$ (s⁻¹)	$k_{cat}/K_{m,NAD+}$ (mM⁻¹s⁻¹)
WT	0.143 ± 0.065	0.208 ± 0.027	1.454	0.223 ± 0.053	0.197 ± 0.011	0.883
[a]E108A	/	/	/	/	/	/
[b]R119A	/	/	/	/	/	/
[a]I121A	/	/	/	/	/	/
W133A	1.060 ± 0.143	0.016 ± 0.004	0.015	0.711 ± 0.271	0.012 ± 0.002	0.017
R135A	0.495 ± 0.052	0.174 ± 0.012	0.351	0.276 ± 0.083	0.122 ± 0.020	0.442
R135W	0.592 ± 0.114	0.092 ± 0.010	0.155	0.705 ± 0.113	0.083 ± 0.025	0.118
[b]G140R	/	/	/	/	/	/
[b]R163Q	/	/	/	/	/	/
[a]R236E	/	/	/	/	/	/
I279A	0.015 ± 0.002	0.013 ± 0.001	0.867	1.187 ± 0.193	0.025 ± 0.006	0.021
[a]H283A	/	/	/	/	/	/

[a] E108A/I121A/R236E/H283A were inactive.
[b] The kinetic parameters of R119A/G140R/R163Q could not be fitted due to low activity.
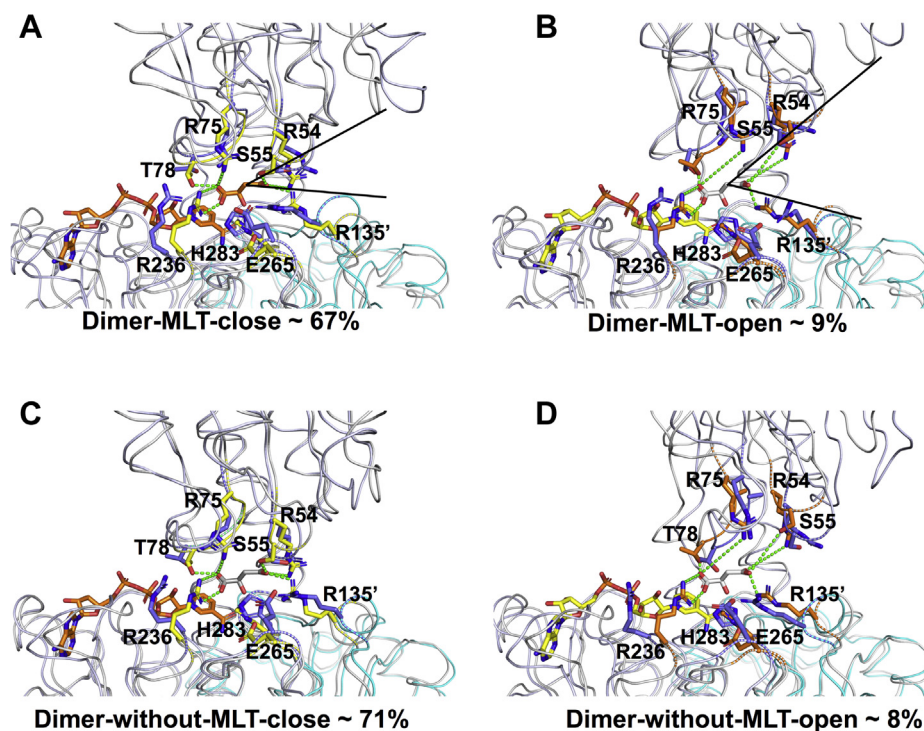
Figure 5. Conformational clusters of the dimer trajectories with or without a substrate analog (MLT). *A* and *B*, the two major clusters observed in the dimer trajectories with MLT correspond to the close and open states. The representative frames (one monomer in *light purple* and the other in *cyan*) of the two clusters are superimposed on top of the crystal structures that represent the close and open states of sPHGDH displaying as gray ribbons (PDB codes: 2G76 and 5N6C). Residues bound to the substrate are shown as *yellow* or *blue sticks* for the crystal structures and frames extracted from MD trajectories, whereas the NAD⁺ and MLT are designated by *orange*. *C* and *D*, present the major clusters obtained in the dimer trajectories without a substrate analog MLT.

which likely facilitates ligand binding (49–51). We observed two major conformational clusters in the dimer trajectories with or without MLT, representing the close or close-like (∼67% or 71%) and open (∼9% or 8%) states, respectively (Fig. 5). However, no substrate-binding-like conformations were observed in the monomeric trajectories. These observed close and open conformations in the dimer trajectories resemble the configurations of sPHGDH crystallized with both a bound cofactor and a substrate analog (L-tartrate) in one monomer and only a bound cofactor in the second monomer (25). In agreement with the structural study, there were no significant conformational changes upon L-tartrate or MLT binding, but the lid domain rotated by ∼ 30° upon substrate binding, and several residues moved into the active site (including R54, S55, and R75) (25). Furthermore, we also noticed that the movements of the catalytic loop (residues 280–288) are coupled with the dimerization loop (residues 120'-145') of the cognate protomer *via* the essential dynamics analysis (Fig. S13). Stable interfacial contacts were observed between the adjacent loop and the catalytic center. In addition, three conserved salt bridges across the dimer interface including E108-R119', E290-K145', and R294-E142' are likely to provide specificity and shape complementarities required for the homodimer formation. These intersubunit contacts may engage in the catalysis by stabilizing the transition-state conformations and facilitate substrate binding.

Influence of sPHGDH interfacial mutations on full-length PHGDH oligomeric state and enzyme activity

We have shown that the interfacial mutants predicted based on the sPHGDH structure disturbed the dimer and the enzyme activity. As the full-length PHGDH contains two additional regulatory domains, we further studied whether or not these mutants could disrupt its oligomeric state and influence the enzyme activity when the regulatory domains are present. We purified the full-length WT PHGDH protein and the mutants (Fig. S3B). All the mutants showed similar CD spectra to the WT protein (Fig. S4B).

We first analyzed the oligomeric state of the full-length PHGDH using AUC. The c(s) distribution profile of WT PHGDH showed three peaks (∼3S, 5S, and 8S) at different concentrations, corresponding to the monomeric, dimeric, and tetrameric states (Fig. 6A). The full-length PHGDH demonstrated similar concentration dependent enzyme activity changes as the sPHGDH does (Fig. 6B). When the enzyme concentrations were 2–6 μM (sPHGDH mainly exists as dimer and PHGDH exists as tetramer), sPHGDH retained about 75% activity of PHGDH. When the enzyme concentrations were below 0.3 μM (the main fraction of sPHGDH is in the monomer state while PHGDH is a dimer), the full-length PHGDH is more active than sPHGDH for about two times (Fig. 6C). These findings indicate that the two regulatory domains also contribute to the enzyme activity.
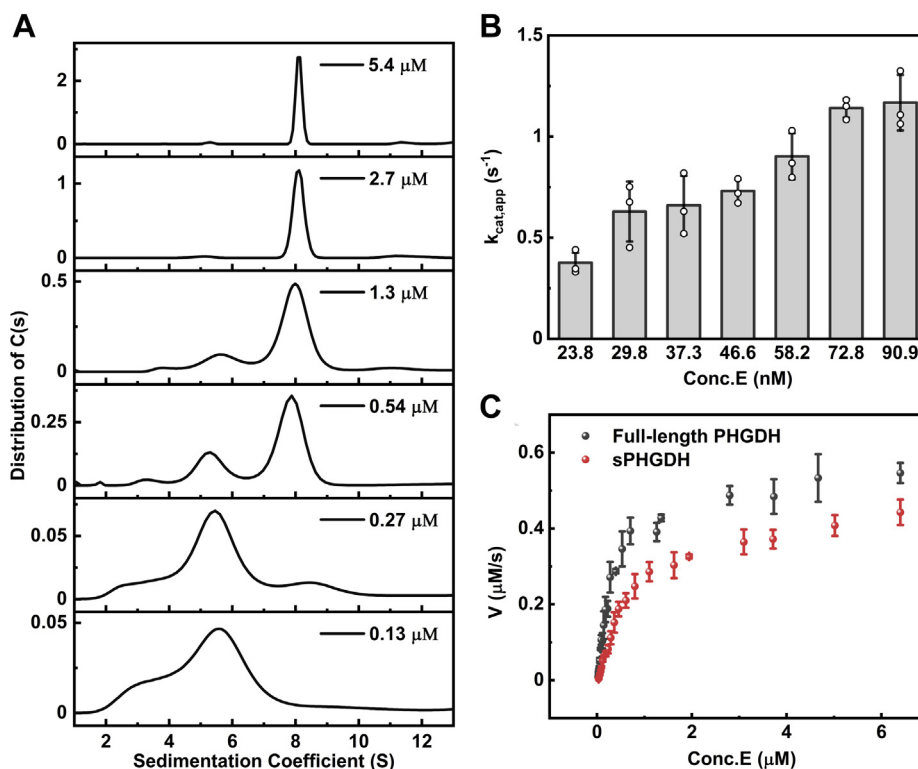
Figure 6. The full-length PHGDH exists as a mixture of tetramers, dimers, and monomers with concentration-dependent enzyme activity. *A*, sedimentation coefficient distribution c(s) profile of PHGDH WT at the indicated concentration. *B*, the catalytic rate constant kcat, app increased with the increased PHGDH WT concentration. *C*, enzyme activity of sPHGDH and PHGDH at different enzyme concentrations (1 mM 3-PG, 1 mM NAD$^+$). *Error bars* represent S.D (n ≥ 3).

We further measured the oligomeric states of all the interfacial mutants in full-length PHGDH. The SEC analysis (Fig. 7A, Table S2) and chemical cross-linking results (Fig. S11, C and D) indicated that E108A, R119A, I121A, and G140R formed smaller oligomers compared with the WT PHGDH. At the concentration of 5.4 μM, sedimentation coefficients of these mutants were ∼5S (Fig. 7B, Table S4), corresponding to dimer. R135A/W and I279A retained similar oligomeric states as PHGDH. W133A and R163Q kept about 60% tetramer. The two active site mutants, R236E and H283A, did not change the oligomeric state as expected. For further understanding about the differences between E108A, R119A, I121A, and G140R, we measured the oligomeric state of these mutants at a lower concentration of 0.27 μM (Fig. 7C). All of them appeared to exist as a mixture of monomer and dimer. Comparing the sedimentation coefficients of the main peaks, the apparent molecular weights of the mutants are in the following order: E108A < I121A < R119A < G140R < R163Q < W133A < R135W < R135A < I279A.

We also measured the enzyme activity of all the full-length PHGDH mutants. At the 0.27 μM protein concentration, E108A and I121A did not show noticeable activity, while the rest of interfacial mutants show significant enzyme activity (Fig. 8, Figs. S15 and S16). When we increased the enzyme concentration to 2.7 μM, E108A and I121A showed weak enzyme activity (Fig. S17). R135W exhibits about fivefold $K_{m,3\text{-PG}}$ value to WT (Table 2) and maintains half of activity as

previous reported (30). Notably, I279A of sPHGDH dissociates into monomers and loses activity, while I279A of the full-length PHGDH retains the original oligomerization state and keeps the enzyme activity. The different behavior of the mutations on sPHGDH and PHGDH implies that the accessory domains may also contribute to stabilize the tetramer by avidity effects (due to the additive effect of two distinct interfaces in the tetramer).

Discussion

In the present study, we analyzed the relationship between the oligomeric states and enzyme activity of the full-length PHGDH and its catalytic unit (sPHGDH). PGDH is present from prokaryotes to human (5). All the three types of PGDH contain a conserved catalytic unit. Prokaryote PGDH only contains the catalytic unit that forms dimer in the reported crystal structures. The crystal structure of sPHGDH was also solved as a dimer. Although the dimer structure was expected to play key role in enzyme catalysis, how it influences the enzyme activity remains elusive. We show that sPHGDH exists as a dimer and monomer mixture in solution and only the dimer form is catalytically active. The apparent enzyme activity of sPHGDH depends on the enzyme concentration used as the dimer proportion varies with the total enzyme concentration. We deduced the catalytic parameter of the sPHGDH dimer, which is not concentration-dependent. As most of the catalytic parameters reported from literatures were apparent
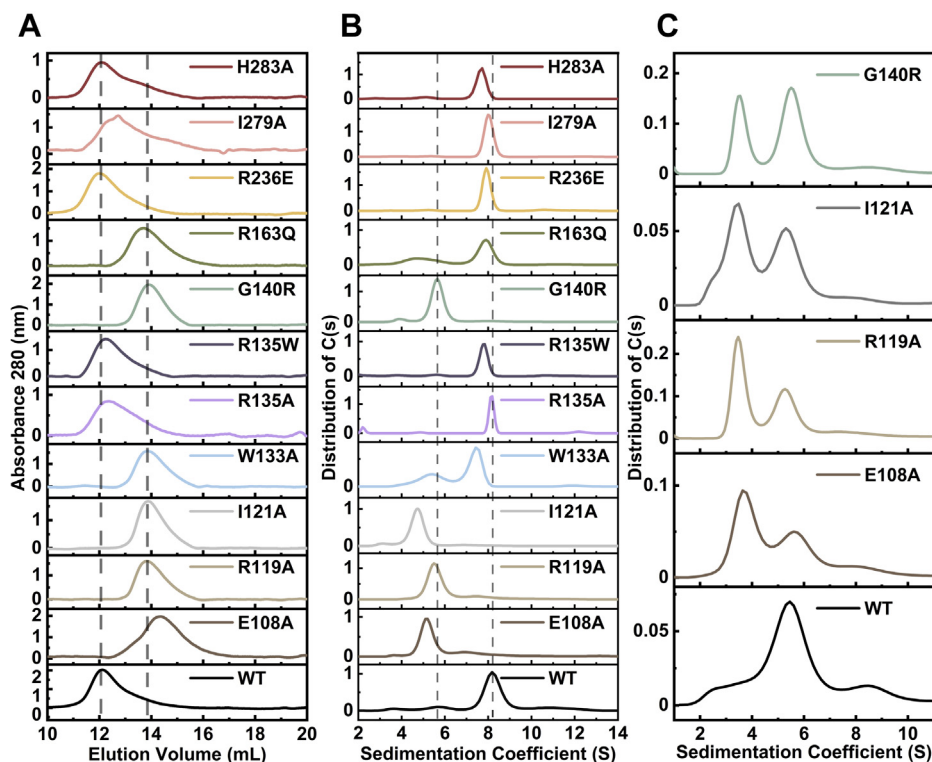
Figure 7. Oligomeric states of the full-length PHGDH and mutants. *A*, size-exclusion chromatograms of PHGDH and mutants at the concentration of 0.3 mg/ml (5.4 μM). *B*, the stack map of sedimentation coefficient distribution c(s) profile of PHGDH and mutants at the concentration of 0.3 mg/ml (5.4 μM). *C*, the stack map of sedimentation coefficient distribution c(s) profile of PHGDH and mutants with a fixed concertation 0.015 mg/ml (0.27 μM). Obvious peak shift of mutants could be observed clearly.

parameters that depend on the enzyme concentration used ([52]), care should be taken when doing comparisons and the enzyme concentrations used should be clearly given.

We analyzed the key residues at the dimer interface of sPHGDH and identified five hotspot residues. Alanine mutations at these sites (E108, R119, I121, W133, and I279) result in inactive monomeric proteins. In the dimeric sPHGDH structure, R135' from the other protomer was found to interact with the substrate 3-PG. It was speculated that R135' may be important in enzyme catalysis by supporting 3-PG binding. Our study shows that the R135A mutant maintains the enzyme activity and the dimer structure with slightly increased $K_{m,3-PG}$,

indicating that the contribution of R135 to the dimer formation is limited. Without R135, the rest of the amino acid residues that interact with 3-PG could still bind the substrate for enzyme catalysis. Formation of the dimer stabilizes the protein structure and makes the protomers take the active conformation required for catalysis.

We show that the full-length PHGDH exists as a mixture of tetramers, dimers, and monomers with a concentration-dependent enzyme activity manner. Both the tetramers and dimers are active. The two regulatory domains do contribute to the enzyme activity as the activity of sPHGDH is about 75% of the full-length PHGDH, which seems to benefit from the
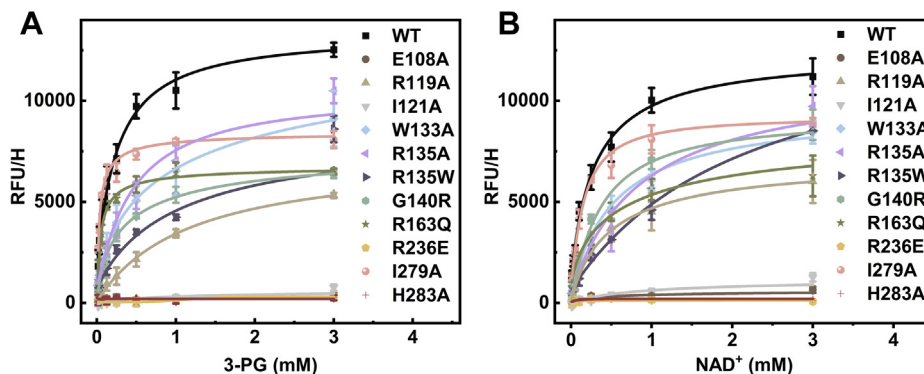

Figure 8. Enzyme reaction kinetics of the full-length PHGDH and mutants. *A*, the reaction kinetics of 0.27 μM PHGDH and mutants with 1 mM NAD$^+$ at different 3-PG concentrations. *B*, the reaction kinetics of 0.27 μM PHGDH and mutants with 1 mM 3-PG at different NAD$^+$ concentrations. *Error bars* represent S.D (n ≥ 3).

Table 2
Kinetic parameters of the full-length PHGDH forward reaction coupled with PSAT1

sPHGDH	$K_{m,3-PG}$ (mM)	$k_{cat, 3-PG}$ (s^{-1})	$k_{cat}/K_{m, 3-PG}$ (mM^{-1}s^{-1})	$K_{m, NAD+}$ (mM)	$k_{cat, NAD+}$ (s^{-1})	$k_{cat}/K_{m,NAD+}$ (mM^{-1}s^{-1})
WT	0.217 ± 0.037	1.163 ± 0.049	5.359	0.287 ± 0.089	1.002 ± 0.113	3.491
[a]E108A	1.958 ± 0.545	0.965 ± 0.120	0.493	1.359 ± 0.366	0.758 ± 0.120	0.558
R119A	1.434 ± 0.294	0.648 ± 0.048	0.452	0.496 ± 0.075	0.574 ± 0.034	1.157
[a]I121A	0.614 ± 0.043	1.286 ± 0.024	2.094	0.987 ± 0.136	1.693 ± 0.078	1.715
W133A	1.447 ± 0.345	1.197 ± 0.093	0.827	0.322 ± 0.078	0.678 ± 0.078	2.105
R135A	0.397 ± 0.087	0.840 ± 0.093	2.116	0.588 ± 0.050	0.971 ± 0.001	1.651
R135W	1.041 ± 0.144	0.691 ± 0.047	0.663	1.561 ± 0.071	1.040 ± 0.021	0.666
G140R	0.346 ± 0.039	0.606 ± 0.021	1.751	0.371 ± 0.077	0.763 ± 0.078	2.057
R163Q	0.054 ± 0.006	0.535 ± 0.013	9.907	0.370 ± 0.101	0.641 ± 0.070	1.732
[b]R236E	/	/	/	/	/	/
I279A	0.034 ± 0.002	0.662 ± 0.014	19.471	0.147 ± 0.024	0.791 ± 0.034	5.381
[b]H283A	/	/	/	/	/	/

[a] The kinetic parameters of full-length E108A and I121A were measured at the tenfold concentrations of WT and other mutants.
[b] R236E and H283A were inactive.

two regulatory domains providing supports and stabilizations of the dimer structure. With the presence of the two regulatory domains, the five hotspot mutants except I279A reduce the size of the oligomers to different extents. I279A retains the oligomeric state with similar activity to the WT PHGDH. As a monomer-dominant mixture of dimers and monomers, R119A maintains about half of the enzyme activity, while E108A and I121A exhibit almost no activity at the enzyme concentration of 0.27 μM. Thus, mutations at E108 and I121 can disrupt the enzyme activity and oligomeric state of the full-length PHGDH. E108 forms salt bridge with R119 to maintain the stable dimer interface (31). I121 is buried in the center of the dimerization interface, forming a hydrophobic cluster with M113' and L109' from the other protomer. E108 and I121 provide key sites for future inhibitor design targeting the oligomeric state of PHGDH.

The two pathogenic mutants G140R and R163Q associated with the lethal NLS1 disease and the PHGDH-deficient mutant R135W all maintain about half of the WT enzyme activity in full-length PHGDH. However, they show different oligomeric states. R135W exhibits a similar tetrameric state as WT PHGDH, while G140R shows a dimeric state and a small fraction of monomer and dimer appears for R163Q at the enzyme concentration of 5.4 μM. This suggests that the severity of the associated genetic diseases is more related to the oligomeric state of the mutant enzyme rather than the catalytic activity. The instability results in increased clearance by protein quality control mechanisms, resulting in much less activity than implied by the activity of a recombinant enzyme. Recently, a number of PHGDH inhibitors have been reported (29, 53–57). Although the NAD$^+$ competitive inhibitors of PHGDH showed nanomolar potency *in vitro*, they work well only under serine deprivation conditions in cellular assays (18). In contrast, moderate inhibition produced by allosteric inhibitors, such as CBR-5884 (58) and disulfiram (DSF) (59) that were shown to disrupt the tetramer structure, is not influenced by environmental serine. Thus, targeting the oligomeric state of PHGDH provides a novel strategy to design drugs that not only inhibit its enzyme activity, but also disrupt other non-catalytic functions yet to be disclosed.

In the present study, we revealed the relationship between the oligomeric state and the activity of PHGDH. Our study provides the first detailed analysis of the hotspot residues at the dimer interface of the PHGDH catalytic unit. We found that single mutations at E108 and I121 can destroy the enzyme activity and oligomeric state of the full-length PHGDH, and these two residues and their nearby residues can be used as novel drug design targeting sites. We showed that the two regulatory domains also contribute the oligomerization and enzyme activity of PHGDH. The full-length PHGDH structure to be solved in the future will provide more information to understand its functional regulation mechanism and provide more sites for drug design.

Experimental procedures

MD simulations and binding free energy calculations

We first used the AnalyseComplex module implemented in FoldX 5 to identify the interface residues on the sPHGDH complex. Next, we employed the PSSM module to mutate each of the interface residues to alanine and calculate the free energy change ($\Delta\Delta G$) of interaction energy upon mutation. This module combines the BuildModel to mutate the residues and the AnalyseComplex to compute the interaction energies (36, 60). MD simulations were performed with the Gromacs package (version 2019) using the Amber99sb-ILDN force field defining the parameters for all residues. The parameters for NAD$^+$ were adopted from JJ Pavelites *et al* 1997, while the parameters for MLT were generated using the Antechamber program implemented in AMBER16 (61). For each simulation, the initial complex structure was placed in a cubic box and intrinsic charges were neutralized using sodium or chloride ions. After 50,000 steps of steepest descent energy minimization, each system was equilibrated using 200 ps of NVT ensemble and 200 ps of NPT ensemble. The equilibrated systems were used for 200 ns or 500 ns full production MD simulations at 300K and 1 bar barostat, with a time step of 2 fs. The atomic coordinates were recorded every 100 ps for further data analysis. Each system was repeated three times to ensure reproducibility. We calculated the binding free energies for the association of the two monomers forming the dimer using the MM-GBSA method of AMBER16 (38). Fifty frames extracted from the last 50 ns from each MD trajectory were used for MM-GBSA calculations. In addition, we extracted structures

between 50 and 500 ns (every 100 ps per structure) for the RMSF, clustering, and essential dynamics analysis.

Protein purification and mutagenesis experiments

The plasmid construction, protein expression, and purification of the C-terminal His6-tagged sPHGDH (1–307), PHGDH (1–533, UniProt: O43175), and PSAT1 (UniProt: Q9Y617) were performed as previously described (56). All mutagenesis experiments were carried out *via* following the instructions of the Quick-Change Site-Directed Mutagenesis (SBS Genetech). In which, the plasmid pET-21a (+)-containing the WT PHGDH was mutated into corresponding variables and then validated using the DNA sequencing approach. Next, the plasmids were transformed to the BL21 (DE3) *E. coli* strain for culturing and purified by nickel-nitrilotriacetic column (HisTrap HP, Cytiva) and gel-filtration column (Sephacryl S-200 HR, Cytiva). For details, see supporting information.

PHGDH enzyme assay

PHGDH activities of the WT and mutants were measured in 96-well plates (100 μl per well) by monitoring the NADH fluorescence as a function of time with a Bioreader (Excitation at 360 nm and Emission at 460 nm). PSAT1 and its substrate glutamate were included to prevent the product inhibition of PHGDH. For details, see supporting information.

Chemical cross-linking experiments

BS3 is a water-soluble, homobifunctional N-hydroxysuccinimide ester (NHS ester). NHS esters react efficiently with primary amino groups (-NH2) in pH 7–9 buffers to form stable amide bonds. The reaction results in the release of N-hydroxysuccinimide. Proteins generally have several primary amines in the side chain of lysine (K) residues and the N-terminus of each polypeptide that are available as targets for NHS-ester reagents. BS3 is a widely used cross-linking reagent, which has been used in PHGDH oligomeric state studies upon treatment of inhibitors CBR-5884 (58) and disulfiram (DSF) (59). sPHGDH (5 μg) or PHGDH (3 μg) and 2.5 mM BS3 (S5799, Sigma) were incubated in 40 mM PBS buffer (pH 7.3) with shaking under the room temperature for 30 min. The reaction was subsequently quenched for 15 min *via* adding 500 mM Tris, pH 7.5, to a final concentration of 45 mM. Then, cross-linked proteins were mixed with the loading buffer, boiled for 10 min, and ran on SDS/PAGE.

Size-exclusion chromatography

Gel filtration experiments were carried out using a Superdex 200,10/300GL column with AKTA FPLC (GE Healthcare). The column was pre-equilibrated and run with 40 mM PBS buffer (pH 7.3, 150 mM NaCl) at a flow rate of 0.6 ml/min. Gel filtration molecular weight markers (β-amylase (200 kD), alcohol dehydrogenase (150 kD), albumin from bovine serum (66 Kd), carbonic anhydrase (29 kD), and cytochrome c (12.4 kD)) were loaded onto the column and calibrated for determining a standard calibration curve based on the retention volumes (Fig. S9). Each of the purified protein samples was loaded 100 μl onto the column with fixed concentration of 0.5 mg/ml (16 μM sPHGDH) or 0.3 mg/ml (5.4 μM full-length PHGDH) for monitoring the eluted volume of the fraction peak at 280 nm.

Analytical ultracentrifugation

Sedimentation velocity experiments were conducted on a Beckman Optima XLA analytical ultracentrifuge equipped with absorbance optics. The proteins were further buffer-exchanged into the sedimentation buffer (40 mM PBS buffer, pH 7.3, 150 mM NaCl). The density of the sedimentation buffer (1.0058 g/ml) and partial specific volume (0.739 ml/g for sPHGDH and 0.744 ml/g for PHGDH) were calculated using the program SEDNTERP (http://www.bbri.org/rasmb/rasmb.html). For sedimentation velocity experiments, 380 μl samples and 400 μl reference solutions were loaded into cells. The rotor temperature was equilibrated at 20 °C with a rotor speed of 50,000 rpm (full-length PHGDH) or 56,000 rpm (sPHGDH). Absorbance scans were collected at 220 nm, 235 nm, or 280 nm. Data were analyzed with Sedfit (freely available at http://www.analyticalultracentrifugation.com).

Data availability

All associated data to the figures and tables are available upon request to the authors.

PHGDH catalytic activity depends on its dimerization

References

1. Zhu, J., and Thompson, C. B. (2019) Metabolic regulation of cell growth and proliferation. *Nat. Rev. Mol. Cell Biol.* **20**, 436–450

2. Locasale, J. W. (2013) Serine, glycine and one-carbon units: Cancer metabolism in full circle. *Nat. Rev. Cancer* **13**, 572–583

3. Yang, M., and Vousden, K. H. (2016) Serine and one-carbon metabolism in cancer. *Nat. Rev. Cancer* **16**, 650–662

4. Yang, J. H., Wada, A., Yoshida, K., Miyoshi, Y., Sayano, T., Esaki, K., Kinoshita, M. O., Tomonaga, S., Azuma, N., Watanabe, M., Hamase, K., Zaitsu, K., Machida, T., Messing, A., Itohara, S., *et al.* (2010) Brain-specific phgdh deletion reveals a pivotal role for L-serine biosynthesis in controlling the level of D-serine, an N-methyl-D-aspartate receptor co-agonist, in adult brain. *J. Biol. Chem.* **285**, 41380–41390

5. Grant, G. A. (2018) D-3-phosphoglycerate dehydrogenase. *Front. Mol. Biosci.* **5**, 1–18

6. Reid, M. A., Allen, A. E., Liu, S., Liberti, M. V., Liu, P., Liu, X., Dai, Z., Gao, X., Wang, Q., Liu, Y., Lai, L., and Locasale, J. W. (2018) Serine synthesis through PHGDH coordinates nucleotide levels by maintaining central carbon metabolism. *Nat. Commun.* **9**, 5442

7. Possemato, R., Marks, K. M., Shaul, Y. D., Pacold, M. E., Kim, D., Birsoy, K., Sethumadhavan, S., Woo, H.-K., Jang, H. G., Jha, A. K., Chen, W. W., Barrett, F. G., Stransky, N., Tsun, Z.-Y., Cowley, G. S., *et al.* (2011) Functional genomics reveal that the serine synthesis pathway is essential in breast cancer. *Nature* **476**, 346–350

8. Locasale, J. W., Grassian, A. R., Melman, T., Lyssiotis, C. A., Mattaini, K. R., Bass, A. J., Heffron, G., Metallo, C. M., Muranen, T., Sharfi, H., Sasaki, A. T., Anastasiou, D., Mullarky, E., Vokes, N. I., Sasaki, M., *et al.* (2011) Phosphoglycerate dehydrogenase diverts glycolytic flux and contributes to oncogenesis. *Nat. Genet.* **43**, 869–874

9. DeNicola, G. M., Chen, P.-H., Mullarky, E., Sudderth, J. A., Hu, Z., Wu, D., Tang, H., Xie, Y., Asara, J. M., Huffman, K. E., Wistuba, I. I., Minna, J. D., DeBerardinis, R. J., and Cantley, L. C. (2015) NRF2 regulates serine biosynthesis in non-small cell lung cancer. *Nat. Genet.* **47**, 1475–1481

10. Liu, J., Guo, S., Li, Q., Yang, L., Xia, Z., Zhang, L., Huang, Z., and Zhang, N. (2013) Phosphoglycerate dehydrogenase induces glioma cells proliferation and invasion by stabilizing forkhead box M1. *J. Neurooncol.* **111**, 245–255

11. Tanner, J. M., Bensard, C., Wei, P., Krah, N. M., Schell, J. C., Gardiner, J., Schiffman, J., Lessnick, S. L., and Rutter, J. (2017) EWS/FLI is a master regulator of metabolic reprogramming in Ewing Sarcoma. *Mol. Cancer Res.* **15**, 1517–1530

12. Song, Z., Feng, C., Lu, Y., Lin, Y., and Dong, C. (2018) PHGDH is an independent prognosis marker and contributes cell proliferation, migration and invasion in human pancreatic cancer. *Gene* **642**, 43–50

13. Yoshino, H., Nohata, N., Miyamoto, K., Yonemori, M., Sakaguchi, T., Sugita, S., Itesako, T., Kofuji, S., Nakagawa, M., Dahiya, R., and Enokida, H. (2017) PHGDH as a key enzyme for serine biosynthesis in HIF2α-targeting therapy for renal cell carcinoma. *Cancer Res.* **77**, 6321–6329

14. Zhang, X., and Bai, W. (2016) Repression of phosphoglycerate dehydrogenase sensitizes triple-negative breast cancer to doxorubicin. *Cancer Chemother. Pharmacol.* **78**, 655–659

15. Ross, K. C., Andrews, A. J., Marion, C. D., Yen, T. J., and Bhattacharjee, V. (2017) Identification of the serine biosynthesis pathway as a critical component of BRAF inhibitor resistance of melanoma, pancreatic, and non-small cell lung cancer cells. *Mol. Cancer Ther.* **16**, 1596–1609

16. Dong, J.-K., Lei, H.-M., Liang, Q., Tang, Y.-B., Zhou, Y., Wang, Y., Zhang, S., Li, W.-B., Tong, Y., Zhuang, G., Zhang, L., Chen, H.-Z., Zhu, L., and Shen, Y. (2018) Overcoming erlotinib resistance in EGFR mutation-positive lung adenocarcinomas through repression of phosphoglycerate dehydrogenase. *Theranostics* **8**, 1808–1823

17. Wei, L., Lee, D., Law, C.-T., Zhang, M. S., Shen, J., Chin, D. W.-C., Zhang, A., Tsang, F. H.-C., Wong, C. L.-S., Ng, I. O.-L., Wong, C. C.-L., and Wong, C.-M. (2019) Genome-wide CRISPR/Cas9 library screening identified PHGDH as a critical driver for Sorafenib resistance in HCC. *Nat. Commun.* **10**, 4681

18. Ngo, B., Kim, E., Osorio-Vasquez, V., Doll, S., Bustraan, S., Liang, R. J., Luengo, A., Davidson, S. M., Ali, A., Ferraro, G. B., Fischer, G. M.,

    Eskandari, R., Kang, D. S., Ni, J., Plasger, A., *et al.* (2020) Limited environmental serine and glycine confer brain metastasis sensitivity to PHGDH inhibition. *Cancer Discov.* **10**, 1352–1373

19. Rathore, R., Schutt, C. R., and Van Tine, B. A. (2020) PHGDH as a mechanism for resistance in metabolically-driven cancers. *Cancer Drug Resist.* **3**, 762–774

20. Matelska, D., Shabalin, I. G., Jabłońska, J., Domagalski, M. J., Kutner, J., Ginalski, K., and Minor, W. (2018) Classification, substrate specificity and structural features of D-2-hydroxyacid dehydrogenases: 2HADH knowledgebase. *BMC Evol. Biol.* **18**, 199

21. Grant, G. A. (2018) D-3-Phosphoglycerate dehydrogenase. *Front. Mol. Biosci.* **5**, 110

22. Lan, X., Chen, S., Salinas, N. D., Tolia, N. H., and Grant, G. A. (2015) Comparison of Type 1 D-3-phosphoglycerate dehydrogenases reveals unique regulation in pathogenic Mycobacteria. *Arch. Biochem. Biophys.* **570**, 32–39

23. Dey, S., Grant, G. A., and Sacchettini, J. C. (2005) Crystal structure of Mycobacterium tuberculosis D-3-phosphoglycerate dehydrogenase: Extreme asymmetry in a tetramer of identical subunits. *J. Biol. Chem.* **280**, 14892–14899

24. Ravez, S., Spillier, Q., Marteau, R., and Feron, O. (2017) Challenges and opportunities in the development of serine synthetic pathway inhibitors for cancer therapy. *J. Med. Chem.* **60**, 1227–1237

25. Unterlass, J. E., Wood, R. J., Baslé, A., Tucker, J., Cano, C., Noble, M. M. E., and Curtin, N. J. (2017) Structural insights into the enzymatic activity and potential substrate promiscuity of human. *Oncotarget* **8**, 104478–104491

26. Mattaini, K. R., Brignole, E. J., Kini, M., Davidson, S. M., Fiske, B. P., Drennan, C. L., and Heiden, M. G. V. (2015) An epitope tag alters phosphoglycerate dehydrogenase structure and impairs ability to support cell proliferation. *Cancer Metab.* **3**, 1–12

27. Marianayagam, N. J., Sunde, M., and Matthews, J. M. (2004) The power of two: Protein dimerization in biology. *Trends Biochem. Sci.* **29**, 618–625

28. Hashimoto, K., and Panchenko, A. R. (2010) Mechanisms of protein oligomerization, the critical role of insertions and deletions in maintaining different oligomeric states. *Proc. Natl. Acad. Sci. U. S. A.* **107**, 20352–20357

29. Weinstabl, H., Treu, M., Rinnenthal, J., Zahn, S. K., Ettmayer, P., Bader, G., Dahmann, G., Kessler, D., Rumpel, K., Mischerikow, N., Savarese, F., Gerstberger, T., Mayer, M., Zoephel, A., Schnitzer, R., *et al.* (2019) Intracellular trapping of the selective phosphoglycerate dehydrogenase (PHGDH) inhibitor BI-4924 disrupts serine biosynthesis. *J. Med. Chem.* **62**, 7976–7997

30. Tabatabaie, L., Koning, T. J. De, Geboers, A. J. J. M., Berg, I. E., Van Den, T., Berger, R., and Klomp, L. W. J.Ã. (2009) Novel mutations in 3-phosphoglycerate dehydrogenase (PHGDH) are distributed throughout the protein and result in altered enzyme kinetics. *Hum. Mutat.* **30**, 749–756

31. Mishra, V., Kumar, A., Ali, V., Nozaki, T., Zhang, K. Y. J., and Bhakuni, V. (2012) Glu-108 is essential for subunit assembly and dimer stability of D-phosphoglycerate dehydrogenase from Entamoeba histolytica. *Mol. Biochem. Parasitol.* **181**, 117–124

32. Grant, G. A., Kim, S. J., Xu, X. L., and Hu, Z. (1999) The contribution of adjacent subunits to the active sites of D-3-phosphoglycerate dehydrogenase. *J. Biol. Chem.* **274**, 5357–5361

33. Grant, G. A., Xu, X. L., and Hu, Z. (2000) Removal of the tryptophan 139 side chain in Escherichia coli D-3-phosphoglycerate dehydrogenase produces a dimeric enzyme without cooperative effects. *Arch. Biochem. Biophys.* **375**, 171–174

34. Kortemme, T., and Baker, D. (2002) A simple physical model for binding energy hot spots in protein-protein complexes. *Proc. Natl. Acad. Sci. U. S. A.* **99**, 14116–14121

35. London, N., Raveh, B., and Schueler-Furman, O. (2013) Druggable protein-protein interactions–from hot spots to hot segments. *Curr. Opin. Chem. Biol.* **17**, 952–959

36. Delgado, J., Radusky, L. G., Cianferoni, D., and Serrano, L. (2019) FoldX 5.0: Working with RNA, small molecules and a new graphical interface. *Bioinformatics* **35**, 4168–4169

37. Huang, P., Chu, S. K. S., Frizzo, H. N., Connolly, M. P., Caster, R. W., and Siegel, J. B. (2020) Evaluating protein engineering thermostability

≋ASBMB

prediction tools using an independently generated dataset. *ACS omega* **5**, 6487–6493

38. Genheden, S., and Ryde, U. (2015) The MM/PBSA and MM/GBSA methods to estimate ligand-binding affinities. *Expert Opin. Drug Discov.* **10**, 449–461

39. Singh, R. K., Raj, I., Pujari, R., and Gourinath, S. (2014) Crystal structures and kinetics of Type III 3-phosphoglycerate dehydrogenase reveal catalysis by lysine. *FEBS J.* **281**, 5498–5512

40. Thompson, J. R., Bell, J. K., Bratt, J., Grant, G. A., and Banaszak, L. J. (2005) Vmax regulation through domain and subunit changes. The active form of phosphoglycerate dehydrogenase. *Biochemistry* **44**, 5763–5773

41. Guharoy, M., and Chakrabarti, P. (2005) Conservation and relative importance of residues across protein-protein interfaces. *Proc. Natl. Acad. Sci. U. S. A.* **102**, 15447–15452

42. Wang, H., Liu, C., and Deng, L. (2018) Enhanced prediction of hot spots at protein-protein interfaces using extreme gradient boosting. *Sci. Rep.* **8**, 14285

43. Halperin, I., Wolfson, H., and Nussinov, R. (2004) Protein-protein interactions; coupling of structurally conserved residues and of hot spots across interfaces. Implications for docking. *Structure* **12**, 1027–1038

44. Hilbert, B. J., Grossman, S. R., Schiffer, C. A., and Royer, W. E. J. (2014) Crystal structures of human CtBP in complex with substrate MTOB reveal active site features useful for inhibitor design. *FEBS Lett.* **588**, 1743–1748

45. Grant, G. A., Lan Xu, X., and Hu, Z. (2004) Quantitative relationships of site to site interaction in Escherichia coli D-3-phosphoglycerate dehydrogenase revealed by asymmetric hybrid tetramers. *J. Biol. Chem.* **279**, 13452–13460

46. Shaheen, R., Rahbeeni, Z., Alhashem, A., Faqeih, E., Zhao, Q., Xiong, Y., Almoisheer, A., Al-qattan, S. M., Almadani, H. A., Al-onazi, N., Al-baqawi, B. S., Saleh, M. A., and Alkuraya, F. S. (2014) Neu-Laxova Syndrome, an inborn error of serine metabolism, is caused by mutations in PHGDH. *Am. J. Hum. Genet.* **94**, 898–904

47. Ruiz-Pernía, J. J., Tuñón, I., Moliner, V., and Allemann, R. K. (2019) Why are some enzymes dimers? Flexibility and catalysis in *Thermotoga maritima* dihydrofolate reductase. *ACS Catal.* **9**, 5902–5911

48. Nishi, H., Hashimoto, K., Madej, T., and Panchenko, A. R. (2013) Evolutionary, physicochemical, and functional mechanisms of protein homooligomerization. *Prog. Mol. Biol. Transl. Sci.* **117**, 3–24

49. Boehr, D. D., Nussinov, R., and Wright, P. E. (2009) The role of dynamic conformational ensembles in biomolecular recognition. *Nat. Chem. Biol.* **5**, 789–796

50. Ma, B., and Nussinov, R. (2010) Enzyme dynamics point to stepwise conformational selection in catalysis. *Curr. Opin. Chem. Biol.* **14**, 652–659

51. Garton, M., MacKinnon, S. S., Malevanets, A., and Wodak, S. J. (2018) Interplay of self-association and conformational flexibility in regulating protein function. *Philos. Trans. R Soc. Lond. B Biol. Sci.* **373**, 20170190

52. Grant, G. A. (2018) Elucidation of a self-sustaining cycle in escherichia coli l-serine biosynthesis that results in the conservation of the coenzyme, NAD⁺. *Biochemistry* **57**, 1798–1806

53. Pacold, M. E., Brimacombe, K. R., Chan, S. H., Rohde, J. M., Lewis, C. A., Swier, L. J. Y. M., Possemato, R., Chen, W. W., Sullivan, L. B., Fiske, B. P., Cho, S., Freinkman, E., Birsoy, K., Abu-Remaileh, M., Shaul, Y. D., *et al.* (2016) A PHGDH inhibitor reveals coordination of serine synthesis and one-carbon unit fate. *Nat. Chem. Biol.* **12**, 452–458

54. Unterlass, J. E., Basle, A., Blackburn, T. J., Tucker, J., Cano, C., Noble, M. E. M., and Curtin, N. J. (2018) Validating and enabling phosphoglycerate dehydrogenase (PHGDH) as a target for fragment-based drug discovery in PHGDH-amplified breast cancer. *Oncotarget* **9**, 13139–13153

55. Ravez, S., Corbet, C., Spillier, Q., Dutu, A., Robin, A. D., Mullarky, E., Cantley, L. C., and Feron, O. (2017) α-Ketothioamide derivatives: A promising tool to interrogate phosphoglycerate dehydrogenase (PHGDH). *J. Med. Chem.* **60**, 1591–1597

56. Wang, Q., Liberti, M. V., Liu, P., Deng, X., Liu, Y., Locasale, J. W., and Lai, L. (2017) Rational design of selective allosteric inhibitors of PHGDH and serine synthesis with anti-tumor activity. *Cell Chem. Biol.* **24**, 55–65

57. Mullarky, E., Xu, J., Robin, A. D., Huggins, D. J., Jennings, A., Noguchi, N., Olland, A., Lakshminarasimhan, D., Miller, M., Tomita, D., Michino, M., Su, T., Zhang, G., Stamford, A. W., Meinke, P. T., *et al.* (2019) Inhibition of 3-phosphoglycerate dehydrogenase (PHGDH) by indole amides abrogates *de novo* serine synthesis in cancer cells. *Bioorg. Med. Chem. Lett.* **29**, 2503–2510

58. Mullarky, E., Lucki, N. C., Beheshti, R., Anglin, J. L., and Gomes, A. P. (2016) Identification of a small molecule inhibitor of 3-phosphoglycerate dehydrogenase to target serine biosynthesis in cancers. *Proc. Natl. Acad. Sci. U. S. A.* **113**, 1778–1783

59. Spillier, Q., Vertommen, D., Ravez, S., Marteau, R., Themans, Q., Corbet, C., Feron, O., Wouters, J., and Frederick, R. (2019) Anti-alcohol abuse drug disulfiram inhibits human PHGDH via disruption of its active tetrameric form through a specific cysteine oxidation. *Sci. Rep.* **9**, 4737

60. Buß, O., Rudat, J., and Ochsenreither, K. (2018) FoldX as protein engineering tool: Better than random based approaches? *Comput. Struct. Biotechnol. J.* **16**, 25–33

61. Hancock, R. D., Reichert, D. E., and Welch, M. J. (1996) Molecular mechanics force field for modeling technetium(V) complexes. *Inorg. Chem.* **35**, 2165–2166